

On Turbulent Fountains with Background Rotation

Andrea M. Lehn

October 15, 2018

1 Introduction

Turbulent fountains are ubiquitous in natural systems as well as in industrial processes [7]. Fountains occur when there is a reversal or arresting of fluid motion due to buoyancy differences between the fluid in the fountain and the ambient environment. A turbulent fountain occurs when a fluid of non-neutral buoyancy is injected from a localized source with sufficient momentum to be driven initially against gravity and to become turbulent. Consider a jet of salty water injected at the bottom of a tank of fresh water. Initially, the salt water will be driven upwards, against gravity, if there is sufficient momentum to make the jet turbulent. The fluid will rise, entraining fresh water along the way, until it can no longer rise. The diluted salty fluid at the top of the fountain then overturns, driven downwards by gravity. The fluid may fall completely to the bottom or intrude horizontally in the ambient if a background density stratification is present.

The role of rotation on the dynamics of turbulent fountains has not been detailed in scientific literature, although it is relevant for geophysical processes. For some natural processes involving turbulent fountains, such as cloud formation or volcanic eruptions, the Earth's rotation may influence the dynamics. This report presents experimental results investigating the role of rotation on turbulent fountains.

1.1 Laminar vs. Turbulent Fountains

The Froude number (Fr) is the non-dimensional group which determines whether or not a fountain will be turbulent or laminar. Consider a circular source with radius R and mean source velocity \bar{u} , injecting buoyant fluid with a modified gravitational acceleration $g' = (\Delta\rho/\rho_0) g$, where $\Delta\rho$ is the density difference between the two fluids, ρ_0 is a reference density, and g is acceleration due to gravity. Fr represents the ratio of inertial forcing to gravitational forcing for the fountain and is defined as

$$Fr = \frac{\bar{u}}{\sqrt{g'R}}. \quad (1)$$

For $Fr \gg 1$ a fountain becomes turbulent while for $Fr = O(1)$ it remains laminar. Qualitatively and quantitatively there are differences between turbulent and laminar fountains. Before overturning, laminar fountains rise to a height, h , which is on the order of R , the source radius. This result may be obtained from dimensional analysis. For a laminar fountain with four variables, h, R, g' and $\bar{u}, h \sim R$ for a source with a fixed g' and \bar{u} . There

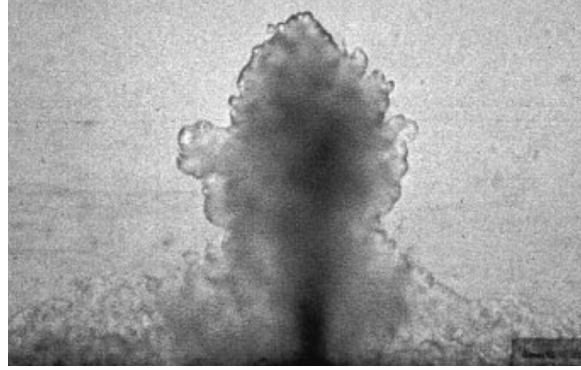


Figure 1: A turbulent fountain rising. Dense, salty water is injected upwards into a fresh ambient from a high Fr source. Image from Bloomfield and Kerr [3].

is little to zero entrainment of the surrounding fluid and the laminar fountain has memory of the source conditions, i.e., the penetration height is totally dependent upon source conditions. Burridge and Hunt [4] have systematically investigated the behavior of fountains at low and very low Fr source values. Overall, these systems are well studied.

The behavior of high Fr sources, i.e. negatively buoyant sources driven by source momentum, was initially studied by Turner in 1966 [8]. Turbulent fountains have little memory of the source conditions due to turbulent entrainment of ambient fluid, which causes the fountain to penetrate such that $h \gg R$. An example of a turbulent fountain is shown in Figure 1. Heavy fluid is injected from a point source upwards into a still body of ambient fluid. Turbulence enhances mixing of the lighter ambient into the injected fluid, which reduces the buoyancy, allowing the fluid to rise higher before overturning and falling back down.

The important parameters for turbulent fountains are the buoyancy flux, B , and the momentum flux, M . M is the volume flux of the source times the mean outlet velocity with units of L^4/T^2 and B is the volume flux of the source times g' , with units of L^4/T^3 . For a source with a circular cross section,

$$M = \pi R^2 \bar{u}^2 \quad (2)$$

and

$$B = \pi R^2 \bar{u} g'. \quad (3)$$

Both of these variables include information about source conditions g' , \bar{u} and R ; however, these parameters alone do not determine the fountain height, as they do for a low Fr source fountain.

Bloomfield and Kerr [3] determined a power law for the mean height of rise of a turbulent fountain, based on original work by Turner [8]. The height, H_f depends solely upon M and B . For a turbulent fountain,

$$H_f = 1.6 M^{3/4} B^{-1/2}. \quad (4)$$

This non-rotating, turbulent H_f is useful as a characteristic length scale. The height of the fountain oscillates about a mean height with relatively large amplitudes. Eddies where

mixing occurs are visible along the sides of the fountain and at the top, as shown in Figure 1. Once the fountain overturns, a curtain partially shields the sides of the rising fountain, preventing the rising fluid from entraining the ambient fluid. The dynamics of turbulent fountains have been well studied for a range of conditions, including turbulent fountains in multi-layer cross-flows [1] and fountains impinging on a density interface [2].

1.2 Low Fr Sources with Rotation

Griffiths and Linden [6] investigated the stability of two-layer density stratified systems with ambient rotation. A curved density interface forms due to the buoyancy difference between the two fluids, and eventually the system becomes unstable under the influence of the Coriolis force. The constant flux experiments performed by Griffiths and Linden are related to the present investigation. A buoyant fluid was injected at the free surface of a homogeneous body of fluid which had been spun-up to rigid body rotation. A circular cross-section, porous source of 1 cm diameter was positioned at the free surface. A constant volume of buoyant fluid was injected for the duration of the experiment, and the radial and vertical growth of a vortex was observed. The Fr values for these experiments are relatively low, ranging from 10^{-3} to 5, so that the flow remains laminar.

A key feature that differentiates the Griffiths and Linden experiments from those presented in this report is that upon injection there is no large vertical penetration of the fluid. For turbulent fountains, there is a large change in height of injected fluid due to source momentum and subsequent entrainment of ambient fluid. The momentum of the source for the Griffiths and Linden experiments, indicated by Fr , is not sufficiently large to create turbulent entrainment of the ambient fluid. In the constant flux experiments, a geostrophic vortex grows, surrounded by the ambient fluid. There is very little mixing. A side-view image showing vertical penetration of a geostrophic vortex is shown in Figure 2.

The streamlines of the flow are solely determined by rotational effects, the Coriolis and centrifugal forces, and the modified gravity, g' , between the two fluids. Eventually, the vortex becomes unstable to rotation and higher order modes occur. A top view of an unstable configuration is shown in Figure 3. The vortex that forms from injected fluid forms a smooth boundary with the ambient fluid since there is negligible mixing at the density interface. The density difference between the two fluids is maintained as the vortex grows. A key result of Griffiths and Linden's work is that the radius, $R \sim t^{1/4}$ and the height, $h \sim t^{1/2}$.

1.3 Objective: Behavior of Turbulent Fountains with Rotation

How the current investigation is situated with published scientific literature can be visualized as table with two options, rotation or no rotation and laminar or turbulent. This grid is shown in Figure 4. Laminar and turbulent fountains have been well characterized and rotating currents with a low Fr have been studied, filling in three quadrants of the grid. Conversely, constant source volume flux, turbulent fountains with background rotation have yet to be studied. This project is situated in the bottom right corner of this grid. The dynamics of the turbulent fountain are studied by systematic experiments over a parameter space determined by important dimensionless groups, as discussed below.

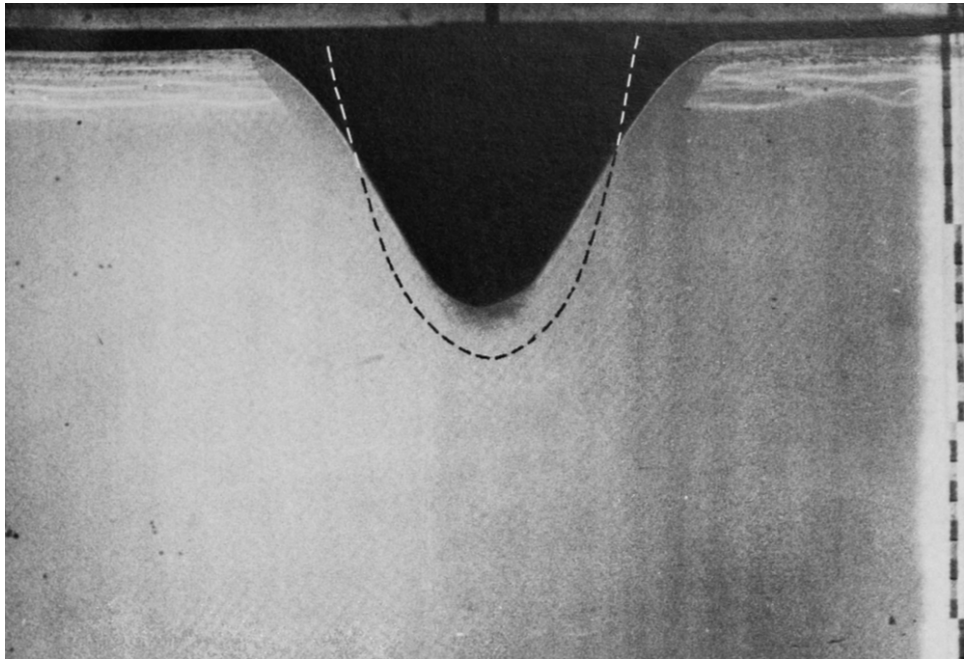


Figure 2: Side view of a vortex forming from Griffiths and Linden [6]. The dark vortex is buoyant fluid injected from a low Fr source. Dotted lines are theoretical predictions of the vortex location. The tank is rotating anti-cyclonically and the vortex is rotating cyclonically.

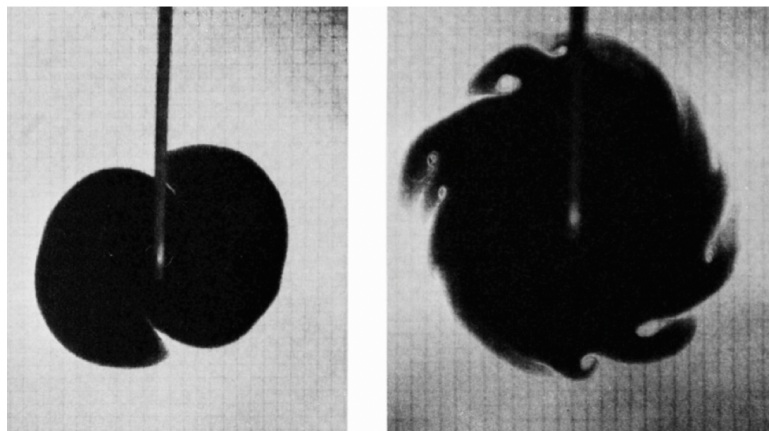


Figure 3: Top view of the onset of instabilities with different azimuthal wave numbers in experiments by Griffiths and Linden [6].

	NON-ROTATING	ROTATING
LAMINAR	<p>Low Fr Fountains</p> <p>Height fluctuation and entrainment of fountains described in literature</p> <p>Burridge and Hunt (2012)</p>	<p>Low Fr Current with Rotation</p> <p>$R_{vortex} \propto t^{1/4}$</p> <p>Griffiths and Linden (1981)</p>
TURBULENT	<p>High Fr Fountain</p> <p>$H = 1.6 M^{3/4} B^{-1/2}$</p> <p>Bloomfield and Kerr (2000)</p> <p>Turner (1966)</p>	<p>High Fr Fountain with Rotation</p> <p>?</p> <p>How do rotation and fountain dynamics interact?</p>

Figure 4: The scientific context of this project fits into the bottom right quadrant of this grid. The dynamics of rotating, turbulent fountains are investigated for the first time in this project.

2 Dimensional Analysis

Dimensional analysis was used to determine a parameter space for experiments. Although dimensional analysis is useful, knowing the relevant physical variables is crucial for determining appropriate dimensionless groups. Based on expected behavior of rotating systems and turbulent fountains, relevant physical variables are determined and scaling is performed to derive three dimensionless Π groups.

Based on the power law produced by Turner [8] and verified by Bloomfield and Kerr [3] there is a time scale for the turbulent fountain. A relevant time scale for the time it takes a fluid parcel to rise to the top of the fountain is the ratio of momentum flux to buoyancy flux, M/B . For a turbulent fountain, recall that momentum flux and buoyancy flux are the relevant parameters for predicting fountain behavior. The Coriolis parameter, f , has units of T^{-1} . It is the appropriate rotational time scale. The Coriolis parameter is equal to twice the rotational frequency of the experimental table: $f = 2\Omega$. In terms of the period of the table's rotation, T_{table} , $\Omega = 2\pi/T_{table}$. Thus, the period of rotation is $4\pi/f$ s.

Since the system is rotating, there is an added stiffness to the fluid due to its vorticity. This can be understood by considering the Taylor-Proudman Theorem. A fluid parcel that is displaced in a direction parallel to the axis of rotation will be forced back to its initial location by rotation. The faster the rotation rate, the more vertical displacement of fluid parcels is suppressed. An alternative argument is that in the limit of rapid rotation, the Taylor-Proudman Theorem gives $\partial w/\partial z = 0$ where w is the velocity in the vertical direction, z . Since there is no vertical flux through the bottom of the tank, $w = 0$, the vertical velocity must be zero everywhere.

Using the Buckingham Pi Theorem and intuition about the system based on the Taylor-Proudman Theorem and on behavior of non-rotating turbulent fountains, three Π groups are determined for the rotating fountain system. There are five relevant variables in the system,

f, M, B , the height of the fountain, H_f and the initial depth of the ambient, H_T . Since there are two dimensions, three Π groups exist. The groups are $\Pi_1 = fM/B$, $\Pi_2 = H_f/H_T$ and $\Pi_3 = M/f^2H_T^4$. The first group, fM/B represents a ratio of the two important time scales of the problem, the fountain rise time to the rotational time. The third group can be thought of as a ratio of the momentum imparted to the fountain and the resistance to vertical penetration. For simplicity, given the time constraint of the GFD program, the ratio of fM/B was varied systematically for fixed values of M . The height of the tank H_T was also fixed. Based on the parameter space, the rotation time scale, $1/f$ was slower than the fountain time scale, M/B . Thus, it was anticipated that the fountain dynamics would dominate the system before rotation.

3 Experimental Setup

3.1 Laboratory Apparatus

Experiments were performed in the Geophysical Fluid Dynamics Laboratory at the Woods Hole Oceanographic Institution. A 91 cm diameter cylindrical plastic tank was placed on a direct-drive rotating table and filled with sea water to $H_T = 35$ cm. A pump was used to inject a constant flux of dyed fluid through a 0.5 cm diameter copper pipe, which was positioned in the center of the tank, just below the free surface. An acrylic lid with a small circular opening for the source was placed on top of the tank for rotating experiments. This was so the air layer above the free surface was also brought up to solid body rotation, to create a nearly stress free boundary between the water and air.

Instrumentation for collecting digital video data from the side view and top view were attached to the rotating table. From the top, a Basler imager was positioned to provide a top view of the entire tank. A Windows machine equipped with software to control the top view camera was mounted to the rotating frame and used to acquire images. Images were collected as single page tifs at a rate of five frames per second. The side view was filmed on a Nikon Coolpix P7000. The collection rate was 24 frames per second. Start times were synchronized using coordinated verbal and visual cues. For the side view, illumination was provided using Light Tape, a flexible electro-luminescent panel, which was aligned flush with the curved tank wall. Pictures of the experimental setup are shown in Figure 5.

3.2 Experimental Parameter Space

A total of 20 experiments were conducted to investigate the role f and B on the behavior of turbulent fountains. The volume flux of the source, Q_0 , M and H_T were fixed at $Q_0 = 5.11$ cm^3/s , $M = 133 \text{ cm}^4/\text{s}^2$ and $H_T = 35$ cm for all experiments. To compare the fountain rise time and rotation time f and B were systematically varied. For the rotating experiments the table was rotated at $f = [0.5, 1.0, 2.0 \text{ and } 3.0] \text{ s}^{-1}$. Another set of experiments examined the non-rotating case, $f=0$. For all five rotation rates, fluids of four different densities were injected to investigate the role of buoyancy. Four values of B were examined, $B/Q_0 = [0, 0.2, 0.5, 1] g'_0$ where $g'_0 \approx 25 \text{ cm}^4\text{s}^{-3}$. The case of $B = 0$ is a jet purely driven by momentum, since there is negligible buoyancy. In terms of the dimensionless parameter fM/B , which represents the ratio of rotational time to fountain rise time, the fountain

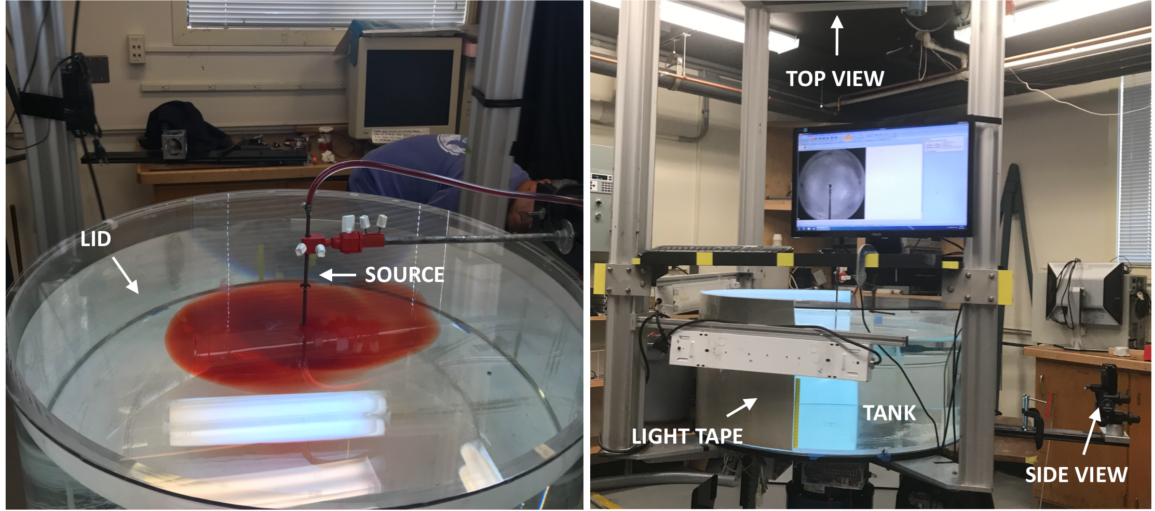


Figure 5: The experimental apparatus used to study rotating fountains. Left: the top view of the rotating system showing the tank lid and source. Right: a side view of the system showing the location of the two camera views as well as the lighting, provided by flexible electro-luminescent lighting (Light Tape).

dynamics are expected to set in before rotation. The Rossby number, Ro is represented by $(fM/B)^{-1}$ for this problem. Ro is a ratio of the rotation time, $1/f$ s to the advective time, M/B s for the initial values of the flow. So, $Ro = B/fM$ for the turbulent fountain with background rotation. The experimental parameter space is shown graphically in Figure 6. The horizontal axis is the reciprocal Ro and the vertical axis is the theoretical fountain height, computed from equation 4, normalized by H_T .

4 Results

4.1 Role of Rotation in Turbulent Fountains

The first experiments were performed by varying f with a fixed B and M . The buoyancy difference was set by the difference between sea water and fresh water, which was the maximum buoyancy flux tested, $B/Q_0 = g'_0$. The role of rotation significantly influences the system dynamics. Figure 7 is a time series comparing a non-rotating turbulent fountain to a turbulent fountain with background rotation. In the non-rotating case, the injected fluid spreads radially as it penetrates the ambient. Billows at the interface of the two fluids indicate turbulent mixing, whereby denser ambient fluid mixes with the fountain, decreasing its buoyancy. With reduced buoyancy, the fountain touches the bottom boundary of the tank and then returns to the surface, driven by buoyancy. The same source conditions with background rotation produced a fountain with a smoother interface and with significantly decreased penetration. The vortex formed in the rotating case prevents the newly injected fluid from mixing with the ambient, thus stifling penetration. Figure 8 shows the fluid interactions occurring in the interior of a surface vortex, formed once the fountain has

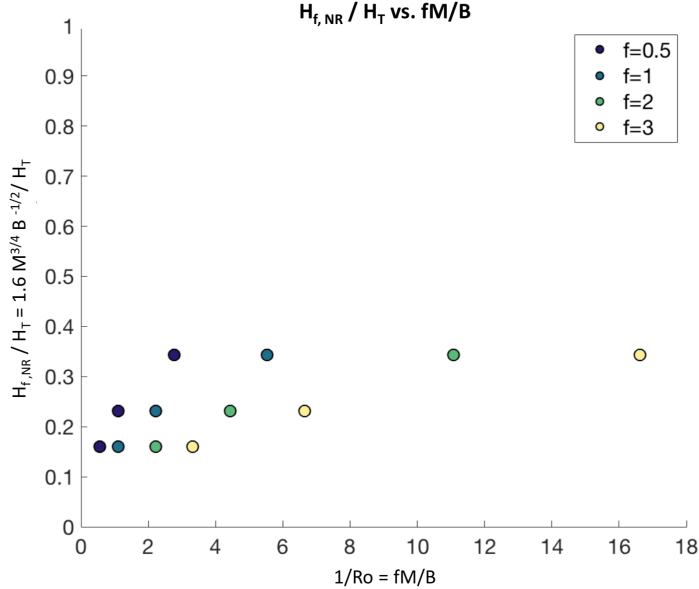


Figure 6: Experimental parameter space for non-zero buoyancy flux and non-zero rotation rate. The vertical axis is H_f based on scaling by Bloomfield and Kerr [3] given in equation 4, scaled by the depth of the ambient, H_T . The horizontal axis is the reciprocal Ro , fM/B .

turned around and risen due to its buoyancy. The injected fluid is initially colored yellow but then dyed red after the vortex has established. The red fluid shows the fountain still exists but is contained within the vortex. A small region at the center of the fountain may punch through the vortex, but largely the fountain is contained within the vortex. Since the newly injected fluid is largely shielded from the ambient by the established vortex, it may only entrain fluid of similar density, leaving its buoyancy relatively unchanged. Without the reduction in buoyancy, the fountain penetrates less deeply. It is too buoyant to continue further and must rise.

For all non-zero rotation rates, rotation systematically decreases the vertical fountain penetration. Figure 9 shows the height of the fountain as a function of time for a fixed value of $B/Q_0 = g'_0$ and four non-zero f values. Data is plotted until a consistent fountain depth is established. As f increases, the initial entrainment and penetration depth are systematically decreased. Before the vortex has begun to shield the incoming fluid from the ambient, entrainment and mixing occur, as in the non-rotating case. The vortex establishes more rapidly at higher f , decreasing the time available for fluid to entrain the denser ambient. Thus, the buoyancy remains unchanged and the fountain does not penetrate as deeply. The average fountain height obtained from data presented in Figure 9, scaled by the height of a non-rotating turbulent fountain, $H_f = 1.6M^{3/4}B^{-1/2}$ is plotted against fM/B in Figure 10. This non-dimensional plot shows that the penetration of the fountain is substantially reduced with increasing rotation. By comparing the volume of the vortex with time to the injected volume, it is clear that rotation systematically suppresses entrainment, as shown in Figure 11. Overall, the entrainment is small relative to the injected volume and only occurs at early times, when the fountain is initiated, before the vortex partially

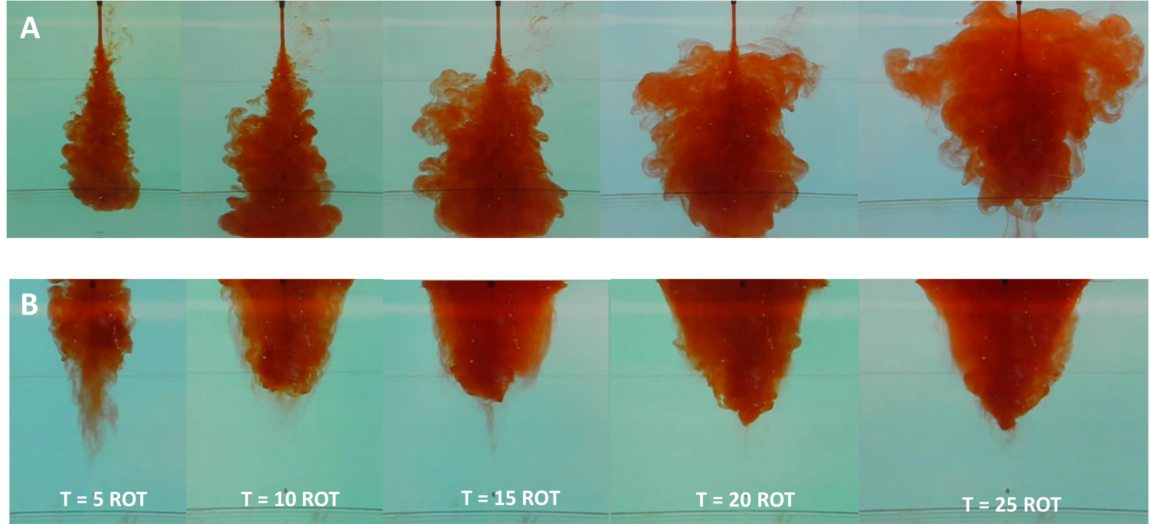


Figure 7: A time series showing the influence of rotation on turbulent fountain dynamics. Panel A shows a turbulent fountain with no background rotation. The fountain becomes turbulent, hits the bottom of the tank, and eventually rises back up to the surface. Panel B shows the same fluid being injected with identical source conditions, $B/Q_0 = 0.5g'_0 = 12.5 \text{ cm}^4\text{s}^{-3}$ and $M = 133 \text{ cm}^4\text{s}^{-2}$, but with a background rotation of $f = 3.0 \text{ s}^{-1}$. The period of one rotation ($T = 1 \text{ ROT}$) was 4.2 s.



Figure 8: A time series revealing fountain behavior in an established vortex. The fountain color is changed from yellow to red after the vortex has established. The interior behavior of the vortex-fountain system is qualitatively shown to be complex, including stratification and circulation. Source conditions were $B/Q_0 = g'_0 = 25 \text{ cm}^4\text{s}^{-3}$ and $M = 133 \text{ cm}^4\text{s}^{-2}$ with a background rotation of $f = 0.5 \text{ s}^{-1}$.

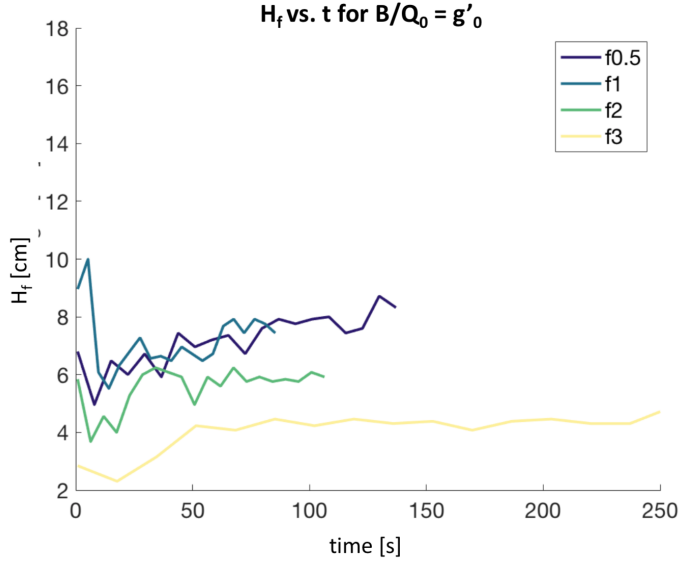


Figure 9: Height of the fountain versus time for increasing f at a fixed B . Source conditions were $B/Q_0 = g'_0 = 25 \text{ cm}^4 \text{s}^{-3}$ and $M = 133 \text{ cm}^4 \text{s}^{-2}$.

encapsulates the fountain. Entrainment of ambient fluid subsidies as more fluid is injected because the fountain is contained within the growing vortex, shown qualitatively in Figure 8. The fountain is entraining fluid of a density close to that of itself, which doesn't enhance mixing with the ambient and maintains a large g' .

Unexpectedly, the radius of the vortex which develops at the surface grows with $t^{1/2}$. A log-log plot of radius versus time is shown for all g' values with varying f in Figure 12. Since this collapses well to a line with slope of a half, this suggests that $R(t) \sim t^{1/2}$. This is robust for all non-zero values of f and B examined. Notably, this behavior is different than the $t^{1/4}$ scaling demonstrated by Griffiths and Linden [6]. A scaling for R as a function of f was estimated by plotting the vertical intercepts of the log-log R vs. t plots and assuming a power law scaling of the form $R \sim t^{1/2}f^\beta$. This power law can be determined by plotting the vertical intercepts of the lines of slope $m = 1/2$, shown as dotted lines on Figure 13. Plotting these vertical intercepts against $\log f$ would produce a line should a power law scaling be correct. Figure 13 shows the intercepts used to determine the value of β . Figure 14 shows the intercepts plotted against $\log f$. Two dotted lines are plotted to serve as visual aids, one of slope $m = -1/3$ and one of $m = -1/2$. A similar approach was applied for the B , using data from cases with varying g' , to find that $R \sim B^{1/3}$.

The power law for $R \sim f^\beta$ is not obvious. There is support for $\beta = -1/3$ and for $\beta = -1/2$, but it is not clear which is correct given the limited amount of data currently available. A value of $\beta = -1/3$ would be consistent with a $-1/3$ power law for the dimensionless group fM/B since $R \sim B^{1/3}$. A linear least squares fit produced a slope of $\beta = -0.44$ with a R-squared error $R^2 = 0.99$ and an RMS error of 0.042. Since there are only four data points, this power law is not yet definitive. However, a power law of $\beta = -0.44$ is consistent with expected values based on dimensional analysis and physical reasoning, as discussed further

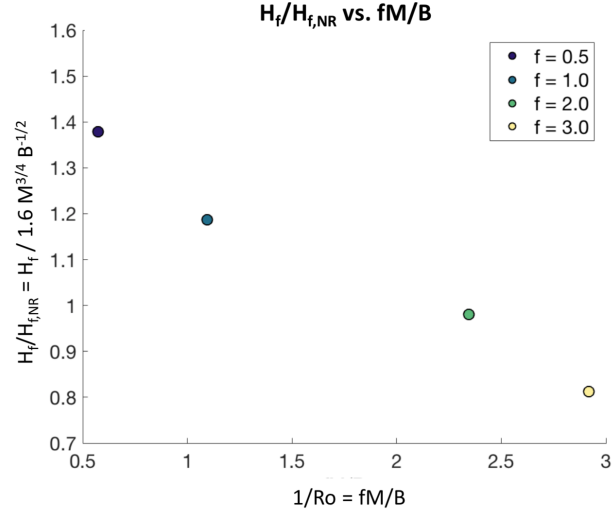


Figure 10: Average fountain height after long times normalized by the non-rotating fountain height, plotted against fM/B for one value of $B/Q_0 = g'_0$. Average H_f values are obtained from data shown Figure 9.

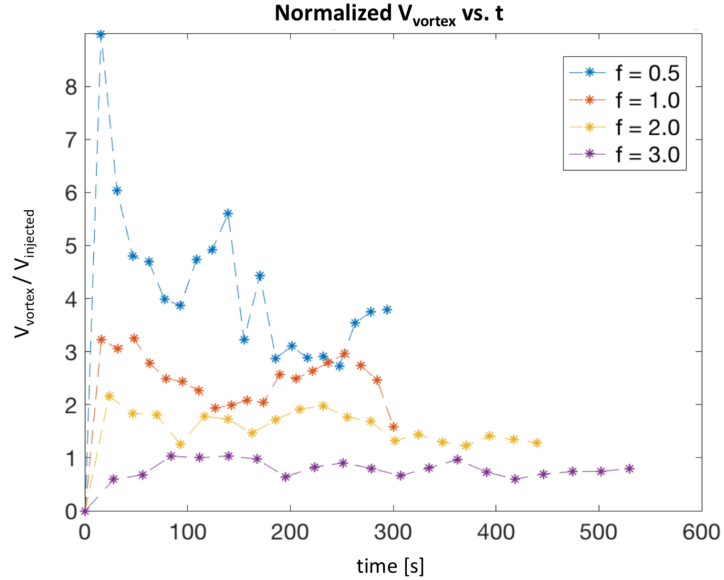


Figure 11: The volume of the vortex that develops plotted against total injected volume as a function of time. The initial entrainment, indicated by the large increase in volume at early times, is decreased with increasing f . Source conditions were $B/Q_0 = g'_0 = 25 \text{ cm}^4 \text{s}^{-3}$ and $M = 133 \text{ cm}^4 \text{s}^{-2}$.

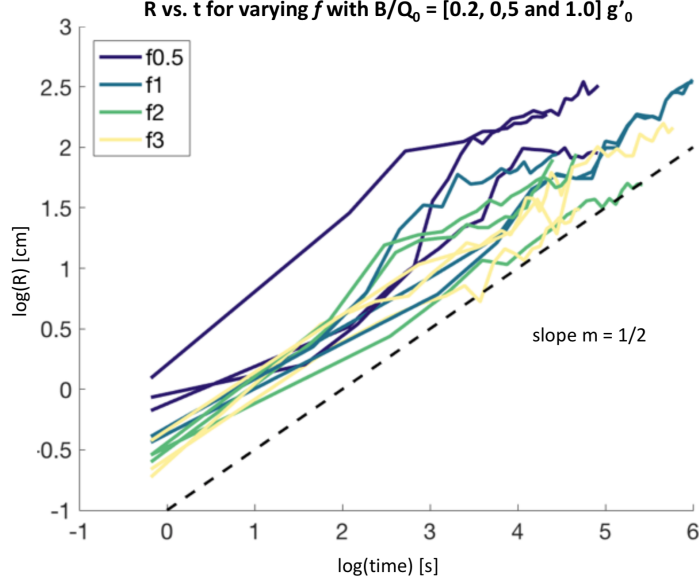


Figure 12: A log-log plot of R vs. t for varying f and three non-zero values of $B/Q_0 = [0.2, 0.5 \text{ and } 1.0] g'_0$ where $g'_0 = 25 \text{ cm}^4\text{s}^{-3}$. A line of slope $m = 1/2$ is shown as a dotted line for comparison to the data. The scaling of $R \sim t^{1/2}$ is robust for the 12 experiments represented here.

in § 4.2.

Plots collapsing the radius according to the scaling relationships $R \sim t^{1/2}B^{1/3}f^{-1/3}$ and $R \sim t^{1/2}B^{1/3}f^{-1/2}$ are presented in Figures 15 and 16, respectively. Both of these plots collapse the data relatively well. Since M and H_T were not varied due to time constraints, there is not enough information to determine a complete scaling for radial growth of the vortex at the surface. However, there has been progress toward determining a comprehensive power law. An interesting finding that is strongly supported by this data set is that the radius grows with $t^{1/2}$ rather than $t^{1/4}$, as was determined by Griffiths and Linden [6].

4.2 Turbulence versus Rotation in Rotating Jets

In order to further understand how rotation impacts the fountain, the simplified case of a pure momentum source (i.e. a jet) with background rotation was studied. The experimental setup was the same, except salt water was injected into salt water, so there was no buoyancy flux. The experiment was repeated for the same rotation rates, $f = [0.5, 1.0, 2.0 \text{ and } 3.0] \text{ s}^{-1}$. As expected from the previous experiments, rotation plays a critical role. A time series of the early time behavior of a jet with and without rotation is shown in Figure 17. The jets subjected to background rotation are contained to a vertical column almost immediately. The non-rotating jet expands laterally and reaches the bottom. Background rotation influences the jet by constraining radial growth to a vertical column. The jet with rotation penetrates the ambient, but does not descend to the bottom of the tank as the jet does. As more fluid is added, the column grows radially and the vertical interface with the ambient fluid is maintained. The fluid appears to be forced into a Taylor column at very

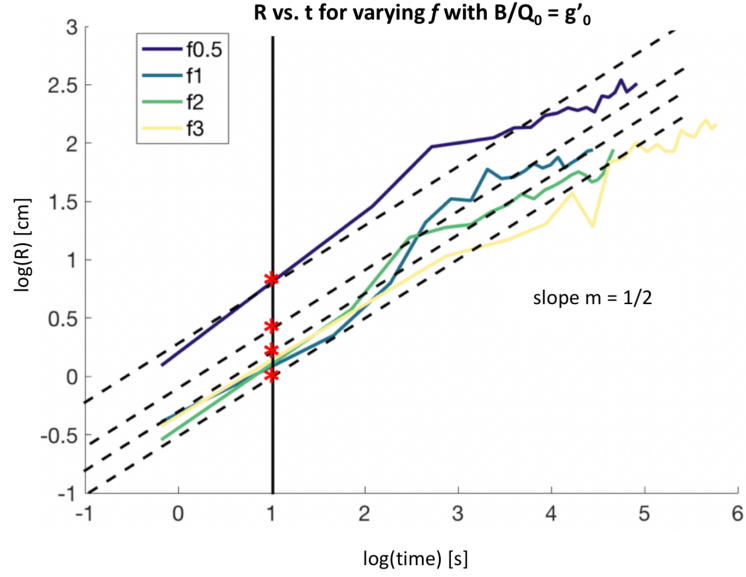


Figure 13: To estimate a power law for $R \sim f^\beta$ the vertical intercepts of the dotted lines, indicated by red asterisks, are plotted against $\log f$ in Figure 14. Source conditions were $B/Q_0 = g'_0 = 25 \text{ cm}^4\text{s}^{-3}$ and $M = 133 \text{ cm}^4\text{s}^{-2}$.

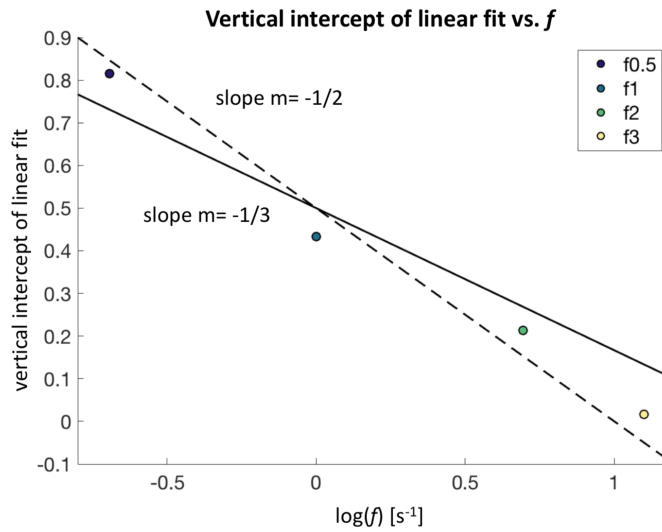


Figure 14: A plot of the vertical intercepts in Figure 13 versus $\log f$. Source conditions were $B/Q_0 = g'_0 = 25 \text{ cm}^4\text{s}^{-3}$ and $M = 133 \text{ cm}^4\text{s}^{-2}$. Lines of slope $m = -1/2$ and $m = -1/3$ are shown for comparison. A least squares analysis produces a slope of $m = -0.44$ with an R-squared fit of $R^2 = 0.99$ and an RMS error of 0.042.

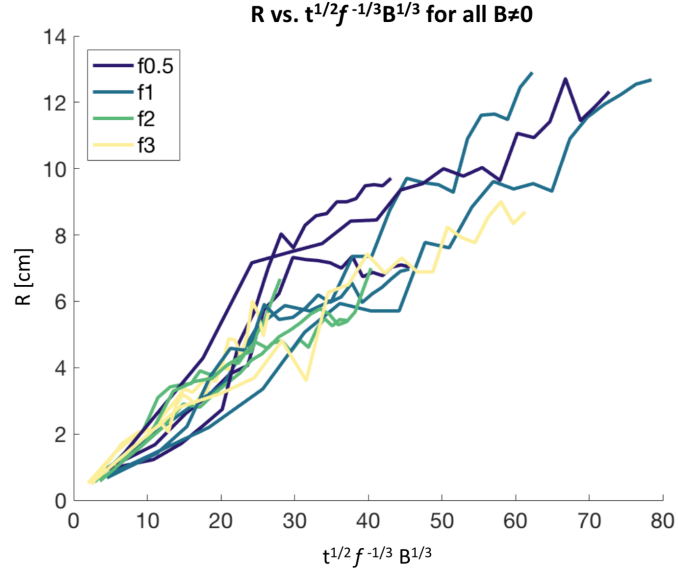


Figure 15: Collapse of R data for cases of non-zero f and B . Data is fit according to the scaling $R \sim t^{1/2}f^{-1/3}B^{1/3}$, which has dimensions of $T^{-1/6}L^{4/3}$. $B/Q_0 = [0.2, 0.5 \text{ and } 1.0]g'_0$ where $g'_0 = 25 \text{ cm}^4\text{s}^{-3}$.

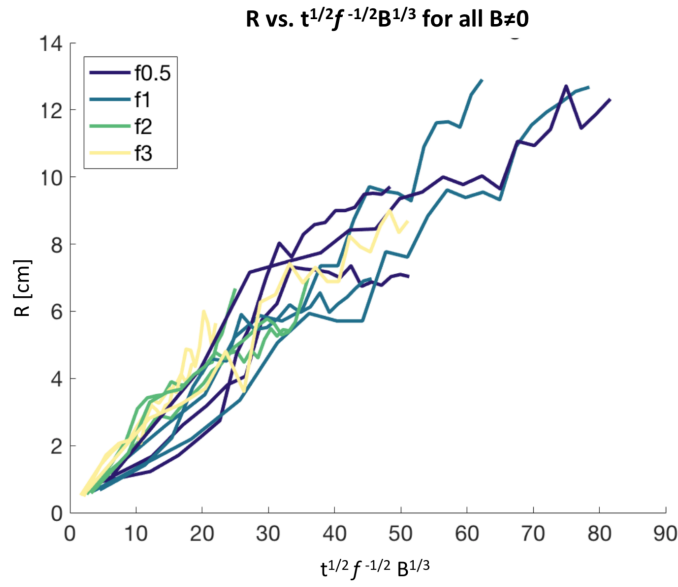


Figure 16: Collapse of R data for cases of non-zero f and B . Data is fit according to the scaling $R \sim t^{1/2}f^{-1/2}B^{1/3}$ which has dimensions of $T^{-1/2}L^{4/3}$. Source conditions were $B/Q_0 = [0.2, 0.5 \text{ and } 1.0]g'_0$ where $g'_0 = 25 \text{ cm}^4\text{s}^{-3}$.

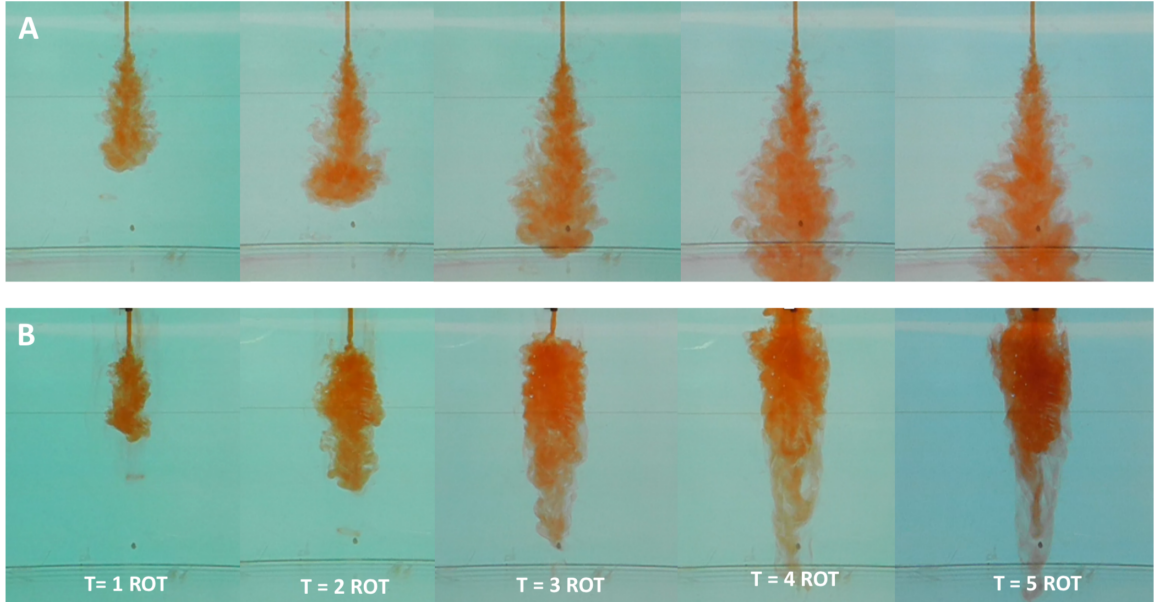


Figure 17: A time series comparing a turbulent jet with no background rotation (A) and with background rotation (B). The rotation rate is $f = 3.0 \text{ s}^{-1}$, corresponding to one rotational period ($T = 1 \text{ ROT}$) of 4.2 s. Snapshots are taken after 1,2,3,4 and 5 rotational periods. Source conditions were $B = 0$ and $M = 133 \text{ cm}^4\text{s}^{-2}$.

early times, as soon as two rotational periods. In order to quantify the role of rotation, the radius of the initial Taylor column, R_{TC} , was plotted against f . An example measurement R_{TC} is shown in Figure 18.

From dimensional analysis an expected scaling for f can be obtained. For a non-buoyant ($B = 0$), turbulent jet with background rotation the meaningful physical parameters are R_{TC} , f , and M . From this, $R_{TC} \sim f^{-1/2} M^{1/4}$ is expected. A dotted line of slope $m = -1/2$ is plotted along with the experimental results in Figure 19. This fits the data well and is consistent with the proposed scaling. A linear least squares analysis yielded a power law exponent of -0.46 with and R-squared error $R^2 = 0.96$ and an RMS error of 0.089. This result agrees with a study of rotating jets by Etling and Fernando, [5]. This scaling of $f^{-1/2}$ may be influencing the radial growth of the vortex for the buoyant cases. This finding supports the scaling of $R \sim f^{-1/2}$, although more data is necessary to validate the relationship.

5 Conclusion and Future Work

The dynamics of turbulent fountains and jets with background rotation was investigated by varying the non-dimensional parameter, fM/B , which represents a ratio of the fountain time to the rotation time. Key results of this project are shown in Figure 20. Although more rigorous statistical analysis is ongoing to clarify and validate the scaling laws presented in this report, many trends have been observed clearly. For cases where $B \neq 0$, once the

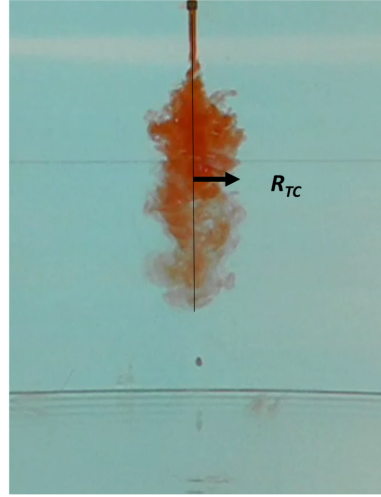


Figure 18: The distance treated as the radius of the Taylor column, R_{TC} , for jets with background rotation. The source conditions were $B = 0$ and $M = 133 \text{ cm}^4\text{s}^{-2}$ with a background rotation of $f = 3.0 \text{ s}^{-1}$.

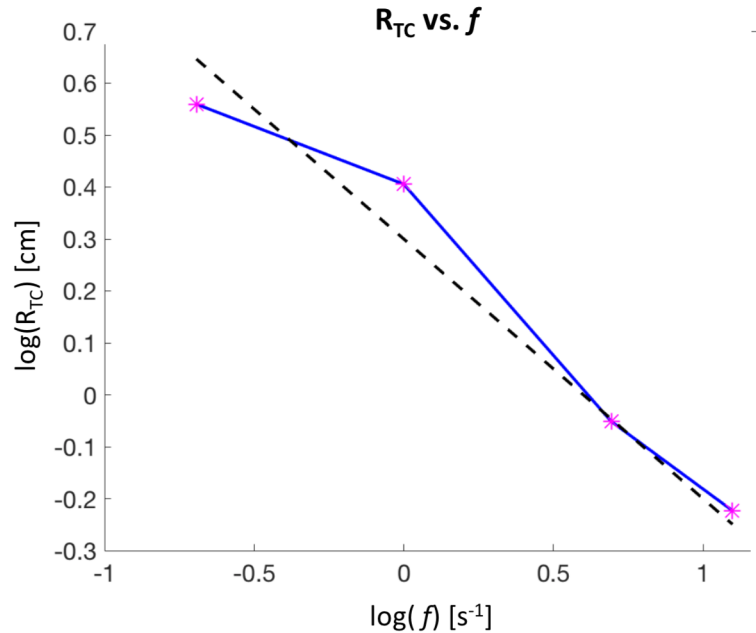


Figure 19: A log-log plot of the radius of the Taylor column versus f . A dotted line of slope $m = -1/2$, which is expected from dimensional analysis, is shown for comparison. The source conditions were $B = 0$ and $M = 133 \text{ cm}^4\text{s}^{-2}$.

	NON-ROTATING	ROTATING
LAMINAR	Low Fr Fountains Height fluctuation and entrainment of fountains described in literature Burridge and Hunt (2012)	Low Fr Current with Rotation $R_{vortex} \propto t^{1/4}$ Griffiths and Linden (1981)
TURBULENT	High Fr Fountain $H = 1.6 M^{3/4} B^{-1/2}$ Bloomfield and Kerr (2000) Turner (1966)	High Fr Fountain with Rotation $R_{vortex} \propto t^{1/2} B^{1/3} f^{-1/3, -1/2}$ $R_{TC} \propto f^{-1/2}$ increasing $f \rightarrow$ decreasing H

Figure 20: As a follow up to the diagram shown in Figure 4, the results of this project have begun to populate the bottom right quadrant.

fountain returns to the surface, the radius of the vortex grows as $R \sim t^{1/2}$. Comparing cases with varying B showed $R \sim B^{1/3}$; however, the dependence on rotation is less clear, leaving $R \sim f^{-1/2}$ and $R \sim f^{-1/3}$ as possible power laws. There is support for both of these laws. More data is necessary to clarify the dependence on f . It could be argued that $R \sim f^{-1/2}$ based on evidence that a Taylor column with $R_{TC} \sim f^{-1/2}$ establishes at early times.

Experiments varying H_T and M will be performed in the near future. H_T appears to matter for the fountain system. This is in contrast to Bloomfield and Kerr [3], where the penetration height H_f does not depend on H_T . Solid-body rotation introduces a stiffness to the ambient fluid which strongly discourages vertical motion, in accordance with the Taylor-Proudman Theorem. This is apparent by how rotation systematically suppresses fountain penetration. The fluid appears to be forced into a Taylor column after just a few rotation periods. R_{TC} appears to scale according to $R_{TC} \sim f^{-1/2}$.

Another ongoing aspect of this project is investigating the onset of instability once the vortex becomes unstable to rotation. A picture demonstrating the onset of different instabilities shown from the top view is show in Figure 21. For a turbulent source with background rotation, higher order azimuthal wave numbers are observed, as they are in Griffiths and Linden [6]. Further characterization of these instabilities will be the topic of future work.

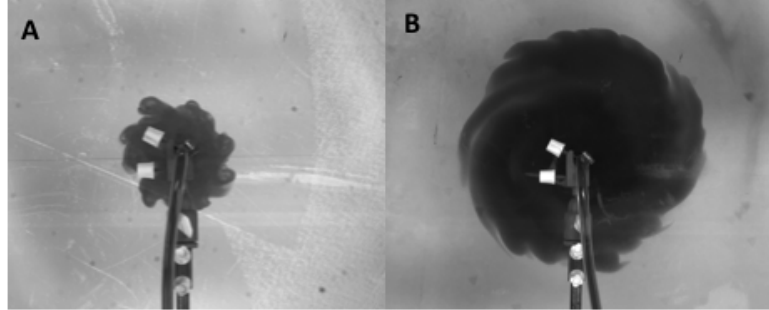


Figure 21: Once the fluid returns to the surface, the vortex becomes unstable to rotation. Characterization of this unstable behavior is ongoing. Panel A shows source conditions of $B/Q_0 = 0.2g'_0 = 4.9 \text{ cm}^4\text{s}^{-3}$ and $M = 133 \text{ cm}^4\text{s}^{-2}$, with a background rotation of $f = 2.0 \text{ s}^{-1}$. Panel B shows source conditions of $B/Q_0 = 0.2g'_0 = 4.9 \text{ cm}^4\text{s}^{-3}$ and the same M with a background rotation of $f = 0.5 \text{ s}^{-1}$.

References

- [1] J. K. ANSONG, A. ANDERSON-FREY, AND B. R. SUTHERLAND, *Turbulent fountains in one- and two-layer crossflows.*, Journal of Fluid Mechanics, 689 (2011), p. 254.
- [2] J. K. ANSONG, P. J. KYBA, AND B. R. SUTHERLAND, *Fountains impinging on a density interface.*, Journal of Fluid Mechanics, 595 (2008), pp. 115 – 139.
- [3] BLOOMFIELD AND KERR, *A theoretical model of a turbulent fountain*, Journal of Fluid Mechanics, 424 (2000), pp. 197–216.
- [4] H. C. BURRIDGE AND G. R. HUNT, *The rise heights of low- and high-froude-number turbulent axisymmetric fountains*, Journal of Fluid Mechanics, 691 (2012), p. 392416.
- [5] D. ETLING AND H. FERNANDO, *On the influence of background rotation on turbulent jets*, Recent Research Advances in the Fluid Mechanics of Turbulent Jets and Plumes, (1994), pp. 401–411.
- [6] R. GRIFFITHS AND P. LINDEN, *The stability of vortices in a rotating, stratified fluid.*, Journal of Fluid Mechanics, 105 (1981), pp. 283 – 316.
- [7] G. HUNT AND H. BURRIDGE, *Fountains in industry and nature*, Annual Review of Fluid Mechanics, 47 (2015), pp. 195–220.
- [8] J. TURNER, *Jets and plumes with negative or reversing buoyancy*, Journal of Fluid Mechanics, 26 (1966), pp. 779 – 792.